Check for updates

ORIGINAL PAPER

Contributory Factors and Distribution Characteristics of Asymmetric Deformation in Deep Tunnel

Yuxue Chen · Mingzhong Gao · Liping Li (iD) **· Shaoshuai Shi · Zongqing Zhou · Mingguang Zhang**

Abstract Aiming at the asymmetric deformation of the surrounding rock in deep tunnels, from the perspective of the mechanical environment of the rock layer, the physical characteristics of the surrounding rock and the geometric characteristics of the tunnel, five kinds of influencing factors for the asymmetric deformation of the tunnel surrounding rock were selected, and the change levels of various factors were established. Through orthogonal test methods, 25 sets of orthogonal test simulation schemes were designed to study the asymmetric deformation law of the surrounding rock of deep roadway under the combined action of various factors. Three surface displacements of the surrounding rock are used as indicators to weigh the influence of various factors on the asymmetric deformation of the surrounding rock. Through the Extreme Difference analysis and F Statistics comparison of the indicators, the dominant influencing factors affect the deformation of the surrounding rock are obtained. By studying the distribution of the maximum deformation position of the surrounding rock, we have obtained the asymmetry characteristics of the surrounding rock deformation. In addition, the simplified mechanical analysis of the key influencing factors of the deformation of the surrounding rock is given, and the distribution law of the asymmetric characteristics of the surrounding rock deformation is summarized. The above research can provide a certain theoretical reference for the asymmetric deformation control and supporting scheme design of the surrounding rock in deep roadway.

Keywords Deep roadway · Asymmetric deformation · Contributory factors · Orthogonal design

Y. Chen · L. Li (✉) · S. Shi · Z. Zhou
School of Qilu Transportation, Shandong University, Jinan, China
e-mail: Zongqing.Zhou@sdu.edu.cn

Y. Chen · L. Li · S. Shi · Z. Zhou
Research Center of Geotechnical and Structural Engineering, Shandong University, Jinan, China

M. Gao
School of Energy and Safety, Anhui University of Science and Technology, Huainan, China

M. Zhang
College of Mining and Safety Engineering, Shandong University of Science and Technology, Qingdao, China

1 Introduction

The increasing demand for energy has forced the exploitation of coal resources to expand into deep

space. When entering deep mining, it has been subjected to complex high ground stress, high ground temperature, high osmotic pressure, mining disturbance (Xie et al. 2019; He et al. 2008; Lamich et al. 2016) and worse stability of the surrounding rock in deep roadway (Zhang et al. 2013), the deformation of the roadway surrounding rock presented the asymmetric deformation characteristics.

Researchers have carried out many studies on the asymmetric deformation failure mechanism and supporting countermeasures of the surrounding rock of the roadway. In the respect of the large deformation and failure mechanism of the deep roadway (Yang et al. 2017; Li et al. 2015), has pointed out the weak position of the roadway surrounding rock and gave the suitable support scheme. Zheng (2010) has summarized that the optimum roadway layout direction should intersect the direction of maximum principal stress with a certain angle which depends on the ratio of principal stresses. Luo et al. (2012) has concluded that the support scheme should aim at the weak position reinforce supported. Chen et al. (2016) has pointed out the deformation of the roof is more serious than that of the sides and floor, and a large zone of relaxation appears around the roadway. Besides, researchers have proposed high-strength supporting system (Wang et al. 2018, 2017), asymmetric reinforced supporting scheme (Wu et al. 2020), and reinforced supporting scheme combined with the site (Song et al. 2019; Wang et al. 2019; Wu et al. 2019; Xu et al. 2017). However, most of the above studies are from the perspective of the force source to support the surrounding rock of the roadway. They only considered the influence of the lithology of the rock layer where the roadway is located (Wu and Qin 2020; Xu et al. 2020). They do not synthetically consider the asymmetric deformation and failure characteristics in terms of the surrounding rock physical characteristics and the roadway geometric features. Preserving the stability in deep roadway not only depends on the physical and mechanical properties of the tunnel layer. Geotechnical characteristics of the overlying rock mass are well known to have a key role in the safety of underground exploitation (Yardimci and Karakus 2020). The overburden layers will also directly affect the stability of the roadway surrounding rock, such as the pillar stability and immediate roof strength are interrelated (Chase et al. 2002), the overburden rigidity contributes to the risk of coal burst because

of dynamic loading by caving in the tunnel layer (Konicek et al. 2013). Studies have shown that the rock hardness of the overlying and underlying rock layers will affect the asymmetric deformation characteristics of the surrounding rock in inclined strata (Chen 2017). In sedimentary formations, the alternating distribution of hard and weak formations is very common, especially in coal measure strata (Wu et al. 2019). Therefore, the lithology and soft–hard distribution relationship of the roof and floor of the tunnel within a certain range have a significant influence on the deformation of the surrounding rock of the deep tunnel.

Deep tunnels are affected by complex stress conditions, combined with the physical characteristics of surrounding rocks and the geometric features of tunnels, the surrounding rocks presents asymmetric deformation. The roadway under complex ground stress conditions can be reflected in the burial depth, the stratum inclination angle and the lateral pressure of the stratum of the roadway (Das et al. 2017). The stress field of the original rock shifted gradually after the excavation of the roadway (Sahendra et al. 2017), and the surrounding rock deformation diversified with the stress environment and the surrounding rock lithology of the roadway. The physical characteristics of the surrounding rock of the roadway could be embodied in the rock layer lithology characteristics. The geometrical characteristics of the roadway are mainly embodied in the roadway excavation shape and the roadway excavation section size. In this paper, for the geometrical characteristics of the roadway, we do not consider the variable roadway section shape, but focus on the semicircle arch roadway under the same width with variable height conditions, which is partly considering the geometrical characteristics.

In summary, for the influencing factors of asymmetrical deformation of surrounding rock, the main factors need to be evaluated, and the asymmetrical characteristics should be determined to target the deformation control study of surrounding rock. Aiming at the problem of asymmetrical deformation in deep roadway, from the aspects of the physical and mechanical characteristics of the surrounding rock and the geometric features of the roadway, we carried out the factors selection which affect the asymmetric deformation. The following five factors were selected: dip angle, lateral pressure coefficient, burial depth, lithology and soft-hard layers location relationship

and height–width ratio. With the orthogonal test method, the key influencing factors of the asymmetric deformation of the roadway surrounding rock were studied. The dominant factors of the amount of deformation of the surrounding rock and the asymmetry features of deformation are obtained, respectively. Besides, the simplified mechanical analysis of the leading factors of deformation and the distribution characteristics of the asymmetry of deformation are given. This research can provide a certain theoretical reference for the design of the surrounding rock support scheme of deep inclined roadways.

2 Contributory Factors Selection and Setting

The change of rock layer dip angle will cause the surrounding rock deformation of deep roadway to present different asymmetric characteristics (Gong et al. 2013; He 2011; He et al. 2015; Sun et al. 2017a, b; Wang et al. 2017). It is necessary to consider the deformation regularity of roadway with the inclination of rock strata. In order to study the influence of the inclination angle on the roadway deformation, five inclination angel levels followed were set up to simulate and compare the deformation. To compare the asymmetric deformation distribution of the roadway, set the $0°$ inclination angle model as reference. Taking the model size effect and boundary effect into consideration and basing on experience, when the size of the model is 3–12 times the size of the roadway, the size effect and boundary effect can be ignored. The roadway width is 5.0 m, so we set the size of the model length and height to be 60 m, the width to be 30 m. The size ratio is in line with the requirements of experience. Meanwhile, the increase in the dip angle of the formation caused the vertical extension of the different formations in the model. To maintain the size ratio between the model and the roadway in the horizontal direction, as the inclination angle increases, the size of the model in the vertical direction also increases. Therefore, the model sizes of $0°$ angel, $15°$ angle and $30°$ angle would have be 60 m long, 30 m width, 60 m height. The $45°$ angle model was 60 m long, 30 m width, 81.2 m height and the $60°$ model with the size of 60 m long, 30 m width, 139.2 m height, shown in Fig. 1. The shape and size of the tunnel cross section will affect the deformation and distribution characteristics of the surrounding rock. In

order to simplify the variation of the section, the fixed arch radius of the roadway is set to 2.5 m, that is, the roadway width is fixed to 5.0 m. Only change the roadway straight wall height, the range of height–width ratio change from 0.7 to 1.1, totally five levels, that is the roadway height change from 3.5 to 6.05 m, shown in Fig. 2a.

As mentioned above, the change of layer lithology and alteration of soft-hard location relationship between the overburden and underlying leaded to diversity deformation and destroy circumstance of the roadway surrounding rock. In the coal sector, the concept of firmness of rock is often used to express the difficulty of rock breaking. The size of the firmness is expressed by the firmness coefficient, also known as the Protodyakonov Scale of Hardness, that is, the f value. We choose three kinds of common lithology, mudstone, sandy mudstone, siltstone, the rock physical parameters were shown in Table 1. Then, the variation range of the f value of the three selected rocks was investigated to measure the rock's soft-hard relationship. When the roadway placed in the soft strata, the relationship between the upper and lower overlying rocks has little influence on the deformation of the roadway surrounding rock (Chen 2017), so simplified the two kinds of lithologic layer relationships of the roadway in the mudstone to one level, therefore, the five kinds of layer relationships were set up as follows Table 2. The burial depth of roadway confirmed to be an important factor affecting the stability of roadway surrounding rock, combined the roadway depth and the lateral pressure coefficient of the strata (Yoo 2016), both set five different levels as shown in Table 3.

3 Orthogonal Design and Analysis of the Asymmetric Deformation

3.1 Orthogonal Scheme Design

Orthogonal design is an efficient experimental design method for arranging multi-factor test and seeking optimal horizontal combination (Hedayat et al. 1999; Sun et al. 2011). Orthogonal design is to select a representative part of the test point (horizontal combination) from the comprehensive test point (horizontal combination) of the optimal area to carry out the experiment, and to understand the situation of the
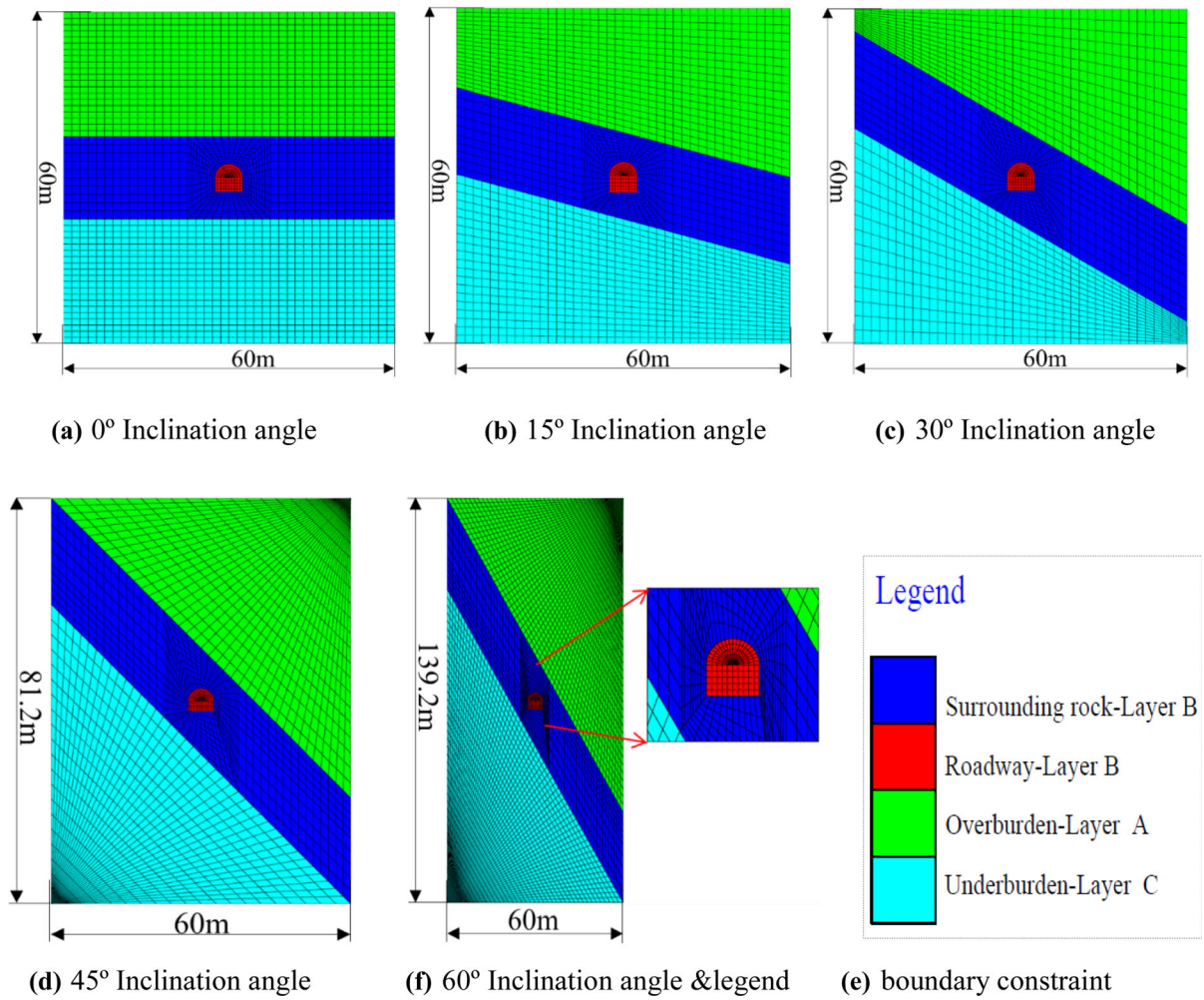
(a) 0° Inclination angle   **(b)** 15° Inclination angle   **(c)** 30° Inclination angle

(d) 45° Inclination angle   **(f)** 60° Inclination angle &legend   **(e)** boundary constraint

Fig. 1 Model diagrams of different strata dip angle levels and boundary constraint

Fig. 2 Tunnel height–width ratio and boundaries

(a) explanation of the height-width ratio   **(b)** model boundary conditions
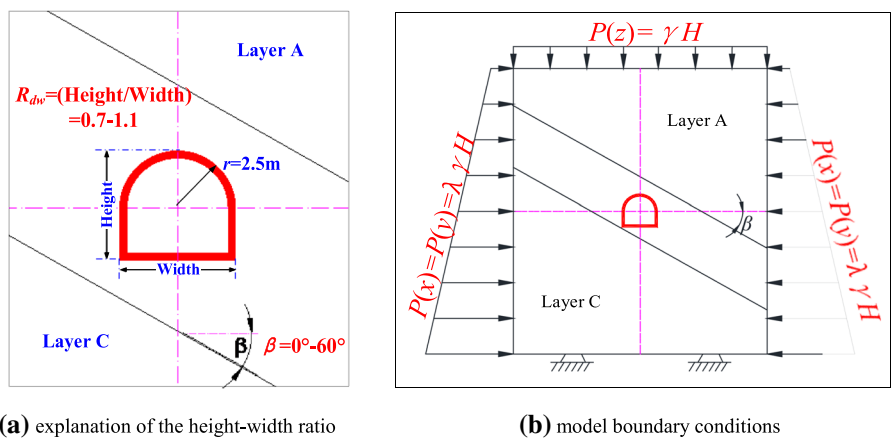
Fig. 3 Orthogonal analysis of roadway maximum surface displacement
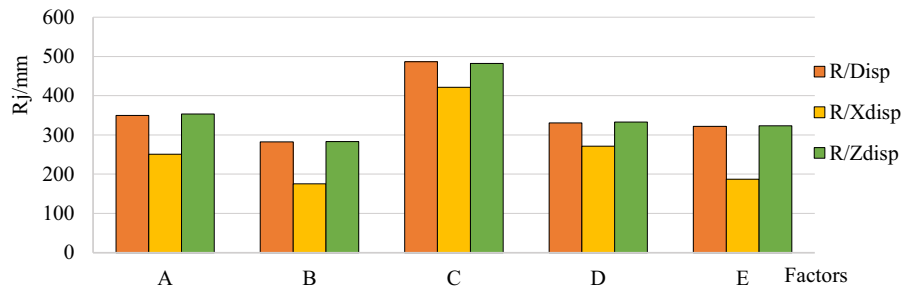

Table 1 Rock physical parameters table

Rock	Unit weight (kN/m³)	Elasticity modulus (GPa)	Poisson's ratio	Tension (MPa)	Cohesion (MPa)	Friction (°)	Protodyakonov scale of hardness	Soft–hard degree
Mudstone	25,950	12.09	0.24	1.39	0.7	32	$1 \sim 3$	Soft
Sandy mudstone	25,650	20.9	0.32	1.82	1.08	37	$3 \sim 4$	Slightly hard
Siltstone	26,400	30.26	0.14	3.73	1.54	40	$4 \sim 7$	Hard

comprehensive test through the analysis of some test results.

From the above, in this paper, we selected five factors affecting the asymmetric deformation of the surrounding rock and set five levels for each factor. In order to accommodate the above factors and their levels, we refer to the orthogonal table (Wang et al. 2013) and select five levels and six factors orthogonal table, namely L25 (5⁶), a total of 25 experiment groups. So the orthogonal table will have a spare column, but this does not affect the orthogonal experimental design in the table. Thus, the F column in the Table 4 named null. The orthogonal test scheme in Table 4 is formed by the design of the table head and the change of each horizontal number in the orthogonal table to the actual horizontal value of

the five influence factors. According to the level of factors in the orthogonal test groups in the table, the experiment was carried out respectively.

As an intuitive and observable measurement, the deformation of surrounding rock surface is used to study the deformation and failure mechanism of tunnel surrounding rock. Here we select the surface deformation of the surrounding rock of the roadway as a measure of asymmetric deformation. We choose three surface displacements as index values of the test design: maximum displacement of roadway surrounding rock (abbreviated to Disp), maximum horizontal displacement of roadway surface (abbreviated to Xdisp) and vertical displacement maximum (abbreviated to Zdisp). According to the orthogonal design scheme, we establish the tunnel numerical model of

Table 2 Lithology and soft-hard layers location relationship levels

No	Layer A	Layer B	Layer C	Levels
1	Sandy mudstone	Mudstone	Siltstone	L0
2	Siltstone	Mudstone	Sandy mudstone	
3	Mudstone	Sandy mudstone	Siltstone	L1
4	Siltstone	Sandy mudstone	Mudstone	L2
5	Mudstone	Siltstone	Sandy mudstone	L3
6	Sandy mudstone	Siltstone	Mudstone	L4

Table 3 Summary of factors levels

Dip angle/°	Lateral pressure coefficient	Burial depth/m	Lithology and soft-hard layers location relationship	Height–width ratio
0°	0.5	100	L0	0.7
15°	0.67	450	L1	0.8
30°	1	800	L2	0.9
45°	1.5	1150	L3	1.0
60°	2.0	1500	L4	1.1

each experimental group respectively. We fixed the around and the lower boundary of all the models and set free boundary at the top of the models, subsequently initial ground stress, shown in Fig. 2b. After tunnel excavation, solve to equilibrium according to the Mohr–Coulomb constitutive model for jointed rock mass damage (Lan et al. 2008). The three index values are recorded and extracted for each test group shown in Table 5.

3.2 Result

After the model was balanced, we traversed the nodes' displacements value of the surrounding rock through a self-define FISH program which embedded in FLAC3D. Then we got the surface maximum displacement (abbreviated to Disp), maximum horizontal displacement (abbreviated to Xdisp), and maximum vertical displacement (abbreviated to Zdisp) of the surrounding rock in each test group (Table 5), and extracted the coordinate positions of each maximum displacement.

It is noteworthy that in most orthogonal test groups, the displacement of roadway surface is mainly based on the vertical displacement deformation. The maximum displacement deformation of roadway surrounding rock surface is vertical deformation. But in the fifth level of the height–width ratio (factor E) of all five orthogonal groups, the distribution of the maximum horizontal displacement of the roadway surrounding rock surface is very close to the distribution of the maximum displacement of the roadway surrounding rock surface. That is, when the roadway height–width ratio is greater than one, the displacement of roadway surface is mainly based on horizontal displacement deformation, and the maximum

displacement deformation of roadway surrounding rock will be transformed into horizontal deformation form.

3.3 Extreme Difference Analysis

For better investigating the investigation index varies with the level change of each factor in all the orthogonal test groups, that is, the selected investigation index with the sensitivity of the factors change, select the Extreme Difference Analysis method (Robin et al. 2016) to analyse the extreme difference of each index value, respectively.

As shown in Fig. 3, the orthogonal analysis diagram of maximum displacement value can show the optimization combination of each factor. R_j is the variance of the j-column factor which reflects the variation of the test index when the level of the factor j is fluctuating. The larger the R_j, the greater the influence of the factor on the test index. According to the magnitude of j, the primary and secondary order of the factor can be judged. The primary and secondary factor affecting the surface maximum displacement can be ordered as: C > A > D > E > B. The primary and secondary factor affecting the surface maximum horizontal displacement can be ordered as: C > D > A > E > B. The primary and secondary factor affecting the surface maximum vertical displacement of the roadway surrounding rock can be ordered as: C > A > D > E > B.

3.4 F statistics—the significance judgement of the factors

The method of extreme error analysis is concise and explicit, with easily data processing and light work load. However, it is not possible to distinguish the data

Table 4 Orthogonal design tests and factors setting

Test groups	Factors					
	A-Dip angle	B-Lateral pressure coefficient	C-Burial depth/(m)	D-Lithology and soft-hard layers location relationship	E-Height–width ratio	F-Null
T1	0°	0.5	100	L0	0.7	0
T2	0°	0.67	800	L3	1.1	1
T3	0°	1	1500	L1	1	2
T4	0°	1.5	450	L4	0.9	3
T5	0°	2	1150	L2	0.8	4
T6	15°	0.5	1500	L3	0.9	4
T7	15°	0.67	450	L1	0.8	0
T8	15°	1	1150	L4	0.7	1
T9	15°	1.5	100	L2	1.1	2
T10	15°	2	800	L0	1	3
T11	30°	0.5	1150	L1	1.1	3
T12	30°	0.67	100	L4	1	4
T13	30°	1	800	L2	0.9	0
T14	30°	1.5	1500	L0	0.8	1
T15	30°	2	450	L3	0.7	2
T16	45°	0.5	800	L4	0.8	2
T17	45°	0.67	1500	L2	0.7	3
T18	45°	1	450	L0	1.1	4
T19	45°	1.5	1150	L3	1	0
T20	45°	2	100	L1	0.9	1
T21	60°	0.5	450	L2	1	1
T22	60°	0.67	1150	L0	0.9	2
T23	60°	1	100	L3	0.8	3
T24	60°	1.5	800	L1	0.7	4
T25	60°	2	1500	L4	1.1	0

fluctuation caused by the condition change or the data fluctuation because of the experimental error. Extreme Difference analysis cannot differentiate the results variance between the different levels was caused by the change in the level of factors, or by the experimental error. Besides, the effect of various factors on the experiment results can't be given a precise quantitative estimate, and it is invalid to put forward only one criterion to determine whether the investigated factors are significant. To make up for the defect of the Extreme Difference Analysis, and decomposing the total data variation into two main parts, factors caused variation and error caused variation, with variance analysis, construct F statistics and make F test, then judge the significance of factors (Mao et al. 2006). F Test, also known as joint hypotheses test, is used to analyse a statistical model

with over one parameter. It can judge whether all or some of the parameters in the model are suitable for estimating the population. The F value is the statistical value of the F test. The F value represents the joint significance between the parameter and the statistical model. When the F value (F_A, F_B, F_C, F_D, F_E) is greater than the relative value of given ($F_{0.05(4,4)} = 6.39$, $F_{0.1(4,4)} = 4.11$) in the orthogonal test, the effect is significant. The larger the F value of the factor, the more significant the effect of the factor on the asymmetric deformation of the surrounding rock. The F test of the surface maximum displacement of the roadway surrounding rock is shown in Fig. 4.

Firstly, refer to F distribution list, the F test results show that the influence of the roadway burial depth (factor C, $F_C = 6.71 > F_{0.05(4,4)} = 6.39$), on the maximum surface displacement of the roadway is

Table 5 Orthogonal design tests indicators

Test groups	Index value/mm		
	Disp	Xdisp	Zdisp
T1	6.31	0.833	6.31
T2	47.45	31.9	47.45
T3	948.921	874.68	948.92
T4	24.88	24.78	21.94
T5	1330.16	803.84	1330.1
T6	115.61	63.44	115.57
T7	50.83	41	49.25
T8	65.57	43.4	65.55
T9	6.834	6.828	4.759
T10	406.82	326.38	406.13
T11	507.89	485.25	417.83
T12	3.165	1.197	3.163
T13	199.64	198.74	198.35
T14	712.11	505.53	712.1
T15	31.52	30.86	24.92
T16	38.39	12.22	38.388
T17	386.81	384.08	386.56
T18	58.34	56.62	53.45
T19	116.31	116.16	105.29
T20	8.165	8.127	4.92
T21	41.53	39	40.74
T22	175.2	132.57	174.15
T23	2.621	1.338	2.614
T24	279.65	190.87	275.23
T25	297.33	297.3	268.23

significant, while the remaining four factors are unremarkable. Secondly, the results of F test show that the influence of the depth (factor C, $F_C = 10.74 > F_{0.05(4,4)} = 6.39$) and lithology and

soft–hard layers location relationship (factor D, $F_D = 4.90 > F_{0.1(4,4)} = 4.11$) on the maximum value of the surface horizontal displacement of the roadway is significant, while the remaining three factors are unremarkable. In addition, the influence of the roadway burial depth (factor C, $F_C = 6.32 > F_{0.1(4,4)} = 4.11$) on the surface vertical displacement of the roadway is significant, the remaining four factors are unremarkable, which is basically in line with the F test of the maximum total surface displacement of the roadway surrounding rock.

For the surface maximum displacement of the surrounding rock, factor C reflects the role of the rock layer mechanical environment, while factor D not only reflects the impact of the physical characteristics of the surrounding rock, but also characterises the impact of geometric features, which is the soft–hard layers location relationship. As the most significant influencing factor of the surrounding rock deformation, it is necessary to carry out theoretical analysis on the force source factors to guide relevant research.

4 Theoretical Calculation

As mentioned, the deformation of surrounding rock is mainly affected by the burial depth of the tunnel, that is, the mechanical environment of the rock layer. Therefore, it is necessary to study the stress environment of the surrounding rock of the tunnel. In engineering, the surrounding rock of the tunnel is often covered with cracks and joints. Affected by layered joints and rock layer inclination, the deformation and failure process of deep inclined roadway exhibits obvious regional asymmetric failure characteristics. According to the deformation and failure

Fig. 4 F statistics of roadway maximum surface displacement. Notes: Refer to F distribution list: $F_{0.05(4,4)} = 6.39$, $F_{0.1(4,4)} = 4.11$
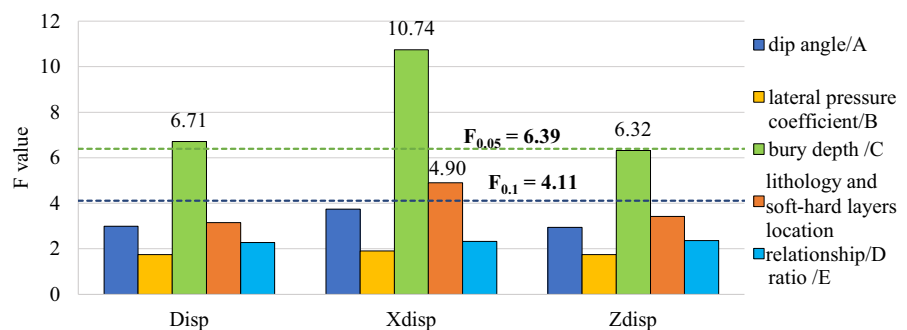
characteristics of the surrounding rock, combined with the occurrence of the stratum and the location of the roadway space, the surrounding rock can be divided into six areas (Fig. 5), where the dip angle is α.

According to the division of the surrounding rock area in Fig. 5, the rock beam model is used to simplify solution. The surrounding rock stress environment of D-I district and D-IV district is similar. The top of the rock beam in D-I district is subjected to a uniformly distributed load, the size is q_1. The bottom is subjected to a linear load which symmetrical about the beam span, and the end size is q_2. The beam end is subjected to an axial load F, the length of the rock beam is L, and the height of the beam is H. It can be regarded as a beam with simply supported ends, which is subjected to uniform and linear loads simultaneously. At the same time, D-II and D-III districts are similar. The top part of the rock beam is subjected to a linear load. The load at the starting end of the cantilever is q_1, the bottom of the rock beam is subjected to a linear load q_2 at the initial section of the cantilever. The length of the cantilever is L, the beam height is H, simplified to a cantilever rock beam subjected to a linear load. D-V district and D-VI district are similar to districts D-II and D-III. The load related to the location and the spatial location of the tunnel, as shown in Fig 6.

The bending moment equation of the rock beam in the D-I district is obtained by the superposition method:

$$M_x = \frac{qL}{2}x - \frac{q}{2}x^2 + \frac{q_2}{4}Lx - \frac{q_2}{3L}x^3 - F\omega \quad (1)$$
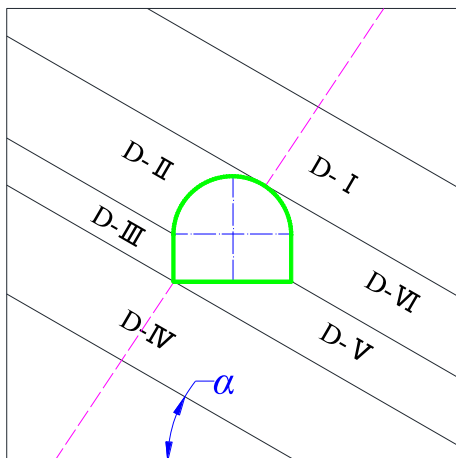

Fig. 5 Districts division of the inclined rock strata

where $q = q_1 - q_2$, ω is the beam deflection.

The position of maximum deflection and maximum bending moment is $x = \frac{L}{2}$, given $F/EI = k^2$,

$$\omega_{max} = \frac{1}{Fk^2}\left(q_1 - \frac{q_1 - q_2}{\cos(kL/2)}\right) + \frac{L^2}{24F}(3q_1 - q_2) \quad (2)$$

$$M_{max} = -\frac{q_1}{k^2}\left(1 - \frac{1}{\cos(kL/2)}\right) \quad (3)$$

Using the semi-inverse solution method, the stress analysis in the D-I district is as follows,

$$\begin{cases} \sigma_x = \frac{6q_1 y}{H^3}\left(\frac{L^2}{4} - x^2\right) + \frac{4q_1}{H^3}y^3 - \frac{3q_1}{5H}y + \frac{4q_2}{LH^3}x^3 y - \frac{8q_2}{LH^3}xy^3 + \frac{6q_2}{5LH}xy - \frac{F}{H} \\ \sigma_y = -\frac{2q_1}{H^3}y^3 + \frac{3q_1}{2H}y - \frac{q_1}{2} + \frac{4q_2}{LH^3}xy^3 - \frac{3q_2}{LH}xy + \frac{q_2}{L}x \\ \tau_{xy} = -\frac{6q_1}{H^3}\left(\frac{H^2}{4} - y^2\right)x - \frac{6q_2}{LH^3}x^2 y^2 + \frac{3q_2}{2LH}x^2 + \frac{2q_2}{LH^3}y^4 - \frac{3q_2}{5LH}y^2 - \frac{q_2 H}{40L} \end{cases} \quad (4)$$

From the similarity, the stress analysis of the D-IV district can be obtained as,

$$\begin{cases} \sigma_x = \frac{6q_2 y}{H^3}\left(\frac{L^2}{4} - x^2\right) + \frac{4q_2}{H^3}y^3 - \frac{3q_2}{5H}y + \frac{4q_1}{LH^3}x^3 y - \frac{8q_1}{LH^3}xy^3 + \frac{6q_1}{5LH}xy - \frac{F}{H} \\ \sigma_y = -\frac{2q_2}{H^3}y^3 + \frac{3q_2}{2H}y - \frac{q_2}{2} + \frac{4q_1}{LH^3}xy^3 - \frac{3q_1}{LH}xy + \frac{q_1}{L}x \\ \tau_{xy} = -\frac{6q_2}{H^3}\left(\frac{H^2}{4} - y^2\right)x - \frac{6q_1}{LH^3}x^2 y^2 + \frac{3q_1}{2LH}x^2 + \frac{2q_1}{LH^3}y^4 - \frac{3q_1}{5LH}y^2 - \frac{q_1 H}{40L} \end{cases} \quad (5)$$

The lower part of the rock beams in the D-II and D-III districts intersect the tunnel excavation surface. With the integration method, we can obtain the deflection curve equation,
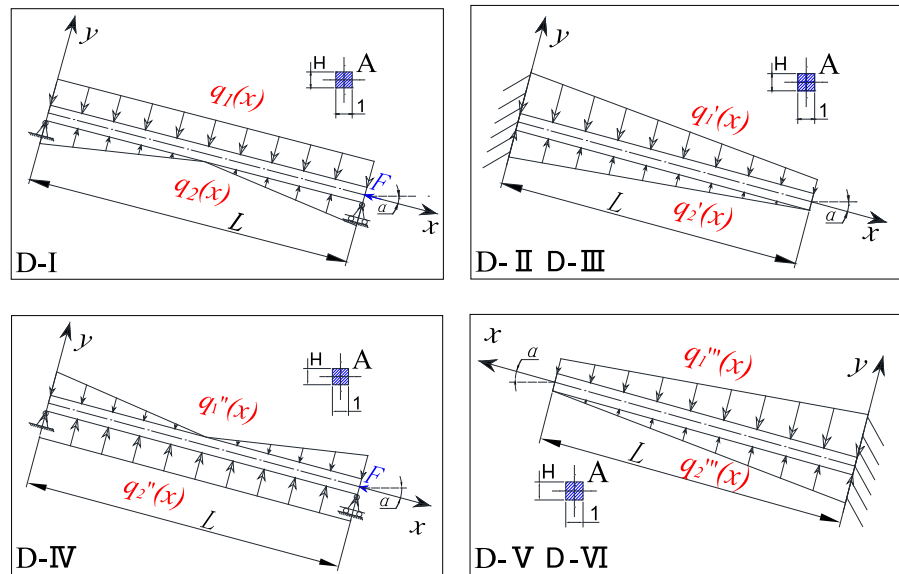
$$\omega_{(x)} = -\frac{q}{120EIL}(L - x)^5 - \frac{qL^3}{24EI}x + \frac{qL^4}{120EI} \quad (6)$$

where $q = q_1 - q_2$, the maximum deflection position is $x = L$,

$$\omega_{max} = -\frac{(q_1 - q_2)L^4}{30EI} \quad (7)$$

the stress analysis by the semi-inverse solution method is,

Fig. 6 Rock beam mechanics models of each district

$$\begin{cases} \sigma_x = \dfrac{q_1 - q_2}{2LH}\left(\dfrac{-x^3 y}{H^2} + \dfrac{4xy^3}{H^2} - \dfrac{3}{5}xy \right) \\[2mm] \sigma_y = \dfrac{q_1 - q_2}{2L}\left(\dfrac{-xy^3}{H^3} + \dfrac{3}{H}xy - x \right) \\[2mm] \tau_{xy} = \dfrac{q_1 - q_2}{LH}\left(\dfrac{3}{H^2}x^2 y^2 - \dfrac{3}{4}x^2 - \dfrac{1}{H^2}y^4 - \dfrac{3}{10}y^2 - \dfrac{H^2}{80} \right) \end{cases}$$
(8)

For D-V district and D-VI district, the simplified assumptions and setting models are basically the same as those in D-II and D-III districts. From the similarity, we can see that the above Eqs. (6)–(8) are also applicable to D-V district and D-VI district.

As mentioned above, the Zdisp of the surrounding rock is the same as the Disp in most orthogonal test groups, but at a higher height–width ratio, the Disp gradually changes to same as the Xdisp, which shows that the height–width ratio will affect the maximum displacement distribution of the surrounding rock. For exploring the asymmetry features distribution laws of surrounding rock deformation under different factors, the location of the maximum deformation distribution of surrounding rock should be studied.

5 Asymmetry Analyses

In horizontal strata, for the straight wall semicircle arch, the roadway surrounding rock surface displacement maximum point, distributes in the roadway vault,

the roadway bottom midpoint and the place of roadway rib department which the arching start at. With the change of strata angle, the maximum point of roadway surface displacement will be changed. In addition, the change of the height–width ratio of the tunnel will also cause the cause the change of the distribution position of the maximum deformation of the surrounding rock. So, the asymmetry of rock deformation in roadway can be measured by the maximum point of displacement of surrounding rock surface. Therefore, we analyse the asymmetry of the surrounding rock deformation through the spatial distributions of the above three displacement indexes.

Due to the setting of the factor roadway height–width ratio among all the orthogonal experimental groups, some changes have taken place in the roadway's contour under this factor, so grouped the displacement index in the test index according to the height–width ratio of the roadway. The location of the maximum value of the surrounding rock displacement may appear on different roadway sections, but based on the plane strain hypothesis, all the spatial distribution points of the maximum value are projected to the $Y = 15$ plane. Then, we plotted the displacement index of each height–width ratio respectively, as shown in Figs. 7, 8, 9, 10 and 11.

As shown in Fig. 7, when the height–width ratio is 0.7, with the change of the strata dip angle, the maximum displacement location points of each surface displacement on the surrounding rock of the
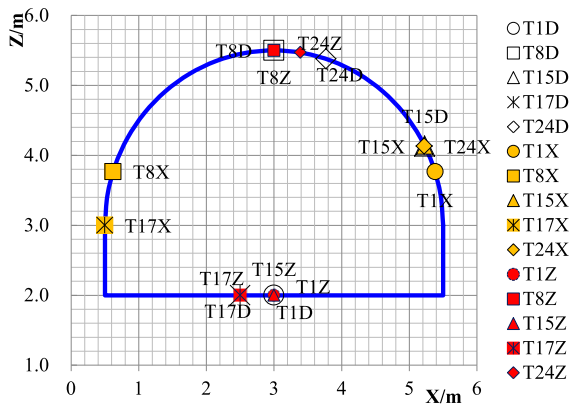
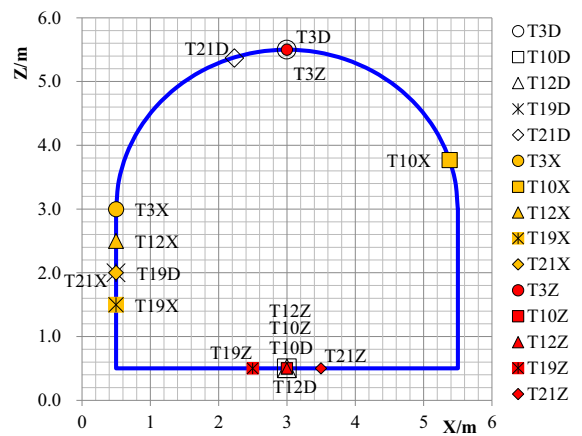**Fig. 7** Displacement index distribution under the height-length ratio 0.7

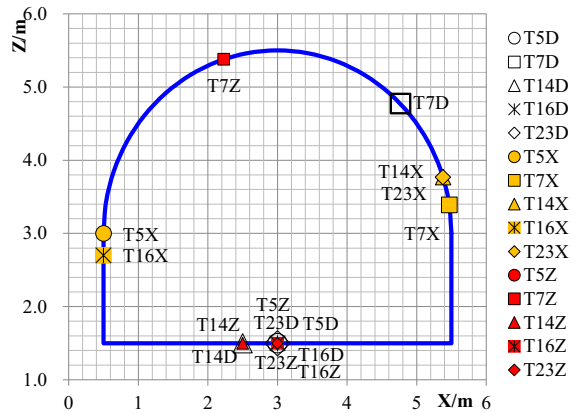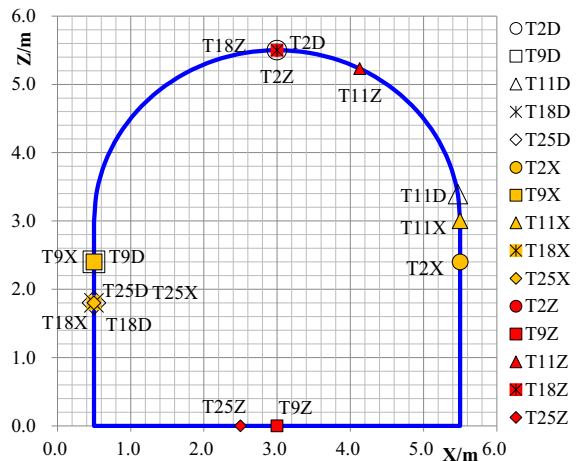**Fig. 8** Displacement index distribution under the height-length ratio 0.8

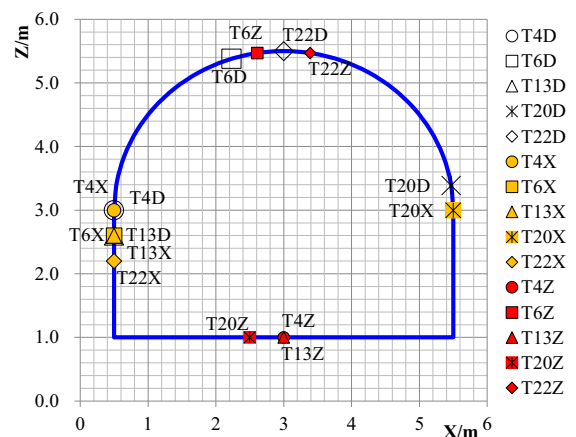**Fig. 9** Displacement index distribution under the height-length ratio 0.9

Fig. 10 Displacement index distribution under the height-length ratio 1.0

Fig. 11 Displacement index distribution under the height-length ratio 1.1

roadway change. In horizontal strata, the Disp and Zdisp locate in the middle position of the bottom of the roadway, while the Xdisp of the roadway surrounding rock does not locate in the arch camber of the roadway section, but in the orthographic projection position of the centre point of the roadway section located on the roadway right rib. Along with the increase of strata dip angle, the position of the Xdisp of the roadway surrounding rock upper and lower deviate from the orthographic projection position of the centre point of the roadway section located on the roadway both ribs. The offset distance increases first and then decreases, When the dip angle is 45°, the maximum offset distance is presented. Meanwhile, the Zdisp of the

roadway surrounding rock will deviate from the tunnel vault or the bottom midpoint, but the deviation phenomenon below the 30° dip angle is unremarkable.

As shown in Fig. 8, when the height–width ratio is 0.8, with the change of strata dip angle, the location of the maximum points of each surface displacement on the roadway surrounding rock are changed. In horizontal strata, the positions of Disp and Zdisp locate at the midpoint of the roadway bottom, and the Xdisp locates in the arch camber of the roadway section, rather than the orthographic projection position of the centre point of the roadway section located on the roadway right rib or the left rib. With the increase of strata dip angle, the positions of Xdisp upper and lower deviate from the position of the Xdisp locations in horizontal strata, while in the 30° and 60° strata dip angle, the deviation is the largest and the deviation in the 45°dip angle is the least. The Zdisp is basically distributed in the midpoint of the bottom of the roadway, except the deviation in 15° dip angle, the deviation is not obvious.

As shown in Fig. 9, when the height–width ratio is 0.9, with the change of strata dip angle, the maximum points of the displacements of the surrounding rock surface change obviously. The majority Disp neither locate in the positions of Zdisp nor locate in the positions of Xdisp. In horizontal strata, the positions of Zdisp locate at the floor midpoint of the roadway (T4Z). The positions of Disp and Xdisp locate in the arch vault of the roadway section (T4D, T4X), instead of locating in orthographic projection position of the centre point of the roadway section located on the roadway right side or the left side. With the increase of dip angle, the positions of Xdisp progressively deviate from the positions of Xdisp in horizontal strata. The offset distance increased gradually except in the 45° dip angle case (T20X). The positions of Zdisp mainly distributed in the midpoint of arch vault or roadway floor. Besides, the deviation of the Zdisp are unremarkable by the five dip angles presented in this paper.

As shown in Fig. 10, when the height–width ratio is 1.0, most of the maximum displacement positions distributed in the roadway up side. In horizontal strata, the Disp and Zdisp located in the vault position of roadway (T3D, T3Z), and the Xdisp located the left arch camber point of the roadway (T3X). With the increase of strata angle, the positions of the Xdisp deviated from the horizontal strata, and the largest offset distance appeared in the 45° dip angle case

(T19X). The positions of Zdisp mainly distributed in the midpoint of the vault or the bottom of the roadway, with unremarkable deviation except the cases of 45° (T19Z) and 60° dip angle (T21Z), the left or the right offset distance distinct changed. That is, when under the 45° dip angle, the position of the maximum displacement of the surrounding rock will show the most significant deviation (T19X, T19Z).

As shown in Fig. 11 when the height–width ratio is 1.1, with the change of the strata dip angle, the maximum point of each displacement in the roadway surrounding rock surface varied gradually. In horizontal strata, the positions of Disp and Zdisp located in the vault of the roadway section, while the position of Xdisp located below the projection position of the roadway section centre point on the down side wall (T2X). At a gently inclined angle ($\alpha = 15$), there is no obvious shift in the location of the maximum displacement distribution of surrounding rock (T9D, T9X, T9Z). With the increase of rock strata dip angle, the position of the Xdisp deviated from the orthographic projection position of the centre point of the roadway section. The offset distance increased with the dip angle, the most apparent deviation phenomenon appeared in the 45° and 60° dip angle case (T18X, T25X). The positions of the Zdisp progressively deviated from the vault or bottom midpoint with the strata dip angle increasing (T11Z, T25Z). Notably, under the 45° dip angle, the positions of the Zdisp didn't present obvious location deviation.

From above, the position of each maximum displacement in the roadway surrounding rock surface varied gradually with the increase of height–width ratio. Under lower height–width ratio, the biggest deviation mainly located in the position of maximum vertical displacement of the surrounding rock. The remarkable deviation mainly appeared in the cases of 45°dip angle and meanwhile affected by the height–width ratio. While the height–width ratio became 1.0 or greater, the biggest deviation mainly located in the position of the maximum horizontal displacement of the surrounding rock, and remarkable deviation mainly appeared in the cases of 45°dip angle. Thus, we should focus on the size of the height–width and the inclination angle when handling the asymmetric deformation of the deep roadway surrounding rock. The distribution law of the three maximum displacement positions can guide the design of the asymmetric

support reinforcement scheme and provide a reference for the reinforcement measures installing position.

6 Conclusions

In order to study the asymmetric deformation characteristics of the surrounding rock in deep roadways, we selected five influencing factors from the mechanical environment of the rock layer, the physical characteristics of the surrounding rock and the geometric characteristics of the tunnel to carry out 25 sets of orthogonal experiments. The asymmetric deformation law of surrounding rock in deep roadway is obtained under the combined action of various factors. The simplified mechanical analysis of the surrounding rock deformation is derived, and the asymmetric deformation distribution characteristics of the surrounding rock are also studied. The main conclusions are as follows:

The roadway burial depth (factor C) dominated the deformation of the deep tunnel roadway surrounding rock. It affected the maximum value of the total displacement, the horizontal displacement and the vertical displacement of the surrounding rock. The primary and secondary factor affecting the surface maximum displacement can be ordered as: C > A > D > E > B.

The lateral pressure coefficient of the strata (factor B) did not show a remarkable influence on the above three deformation. The lithology and soft-hard layers location relationship between the strata (factor D) showed well-marked significance than the other three contributory factors on the horizontal displacement of the surrounding rock. The asymmetric deformation analysis of various factors showed that dip angle of the strata (factor A) and height–width ratio (factor E) have significant influence on the asymmetric deformation. The maximum point of the surrounding rock surface of roadway changed with the change of the dip angle of the rock strata, and gradually deviated from the maximum distribution point under the horizontal strata, and prominently affected by the height–width ratio of the roadway at the same time.

The above research can provide a certain theoretical reference for the asymmetric deformation control and supporting scheme design of the surrounding rock in deep roadway.

References

Chase FE, Mark C, Heasley KA. (2002) Deep cover pillar extraction in the U. S. Coalfields. In: Proceedings of the 21st international conference on ground control in mining. West Virginia: Morgantown, pp 68–80.

Chen M, Yang SQ, Zhang YC, Zang CW (2016) Analysis of the failure mechanism and support technology for the Dongtan deep coal roadway. Geomech Eng 11:401–420

Chen YX (2017) Influence of lithological characters and location on tunnel asymmetric deformation. Safety Coal Mines 48:179–182 (in Chinese)

Das AJ, Mandal PK, Bhattacharjee R, Tiwari S, Kushwaha A, Roy LB (2017) Evaluation of stability of underground workings for exploitation of an inclined coal seam by the ubiquitous joint model. Int J Rock Mech Min Sci 93:101–114

Gong WL, Wang J, Gong YX, Guo PY (2013) Thermography analysis of a roadway excavation experiment in 60° inclined stratified rocks. Int J Rock Mech Min Sci 60:134–147

He MC (2011) Physical modeling of an underground roadway excavation in geologically 45° inclined rock using infrared thermography. Eng Geol 121:165–176

He MC, Wang XY, Liu WT, Yang SB (2008) Numerical simulation on asymmetric deformation of deep soft rock roadway in Kongzhuang Coal Mine. Chin J Rock Mech Eng 27(4):673–678 (in Chinese)

He MC, Peng YY, Zhao SY, Shi HY, Wang N, Gong WL (2015) Fracture mechanism of inversed trapezoidal shaped tunnel excavated in 45 degrees inclined rock strata. Int J Min Sci Technol 25(4):531–535

Hedayat AS, Sloane NA, Stufken J (1999) Orthogonal arrays: theory and applications. Springer-Verlag, New York

Konicek P, Soucek K, Stas L, Singh R (2013) Long-hole destress blasting for rockburst control during deep underground coal mining. Int J Rock Mech Min Sci 61(504):141–153

Lamich D, Marschalko M, Yilmaz I, Bednarova P, Niemiec D, Kubecka K, Mikulenka V (2016) Subsidence measurements in roads and implementation in land use plan optimisation in areas affected by deep coal mining. Environ Earth Sci 75:1–11

Lan H, Yao J, Zhang H, Xu N (2008) Development and application of constitutive model of jointed rock mass damage due to mining based on FLAC3D. Chin J Rock Mech Eng 27:572–579 (in Chinese)

Li LP, Sun SQ, Wang J, Yang WM, Song SG, Fang ZD (2020) Experimental study of the precursor information of the water inrush in shield tunnels due to the proximity of a water-filled cave. Int J Rock Mech Min Sci 130:104320

Li SC, Wang Q, Wang HT, Jiang B, Wang DC, Zhang B, Li Y, Ruan GQ (2015) Model test study on surrounding rock deformation and failure mechanisms of deep roadways with thick top coal. Tun Un Space Tech 47:52–63

Luo F, Yang BS, Sun LH, Yang WB, Cui JK, Zhang L (2012) Experimental research on the failure characteristics of surrounding rock under high vertical ground stress. J Min Safe Eng 29(4):497–504 (in Chinese)

Mao SS, Wang JL, Pu XL (2006) Higher mathematical statistics, 2nd edn. Higher Education Press, Beijing (in Chinese)

Bruyndonckx R, Aerts M, Hens N (2016) Simulation-based evaluation of the performance of the F test in a linear multilevel model setting with sparseness at the level of the primary unit. Biometrical J 58(5):1054–1070

Ram S, Kumar D, Singh AK, Kumar A, Singh R (2017) Field and numerical modelling studies for an efficient placement of roof bolts as breaker line support. Int J Rock Mech Min Sci 93:152–162

Satici O, Unver B (2015) Assessment of tunnel portal stability at jointed rock mass: a comparative case study. Comput Geotec 64:72–82

Song SG, Li SC, Li LP, Shi SS, Zhou ZQ, Liu ZH, Shang CS, Sun HZ (2019) Model test study on vibration blasting of large cross-section tunnel with small clearance in horizontal stratified surrounding rock. Tunn Undergr Sp Tech 92:103013

Sun FS, Pang F, Liu MQ (2011) Construction of column-orthogonal designs for computer experiments. Sci China Math 54(12):2683–2692

Sun XM, Chen F, He MC, Gong WL, Xu HC, Lu H (2017a) Physical modeling of floor heave for the deep-buried roadway excavated in ten degree inclined strata using infrared thermal imaging technology. Tunn Undergr Space Technol 63:228–243

Sun XM, Han Q, Zhang YQ, Liu X, Gong WL (2017b) Experimental investigation of laws during deformation of circular roadway in 10 degrees inclined layered rock. Adv Mater Sci Eng 2017:3503602

Wang J, Chen BS, Fang JH, Wu J, Mei L (2013) The influence of environment factors on lubricants biodegradation by orthogonal design. Advan Mat Res 772:319–322

Wang M, Zheng D, Niu S, Li W (2019) Large deformation of tunnels in longwall coal mines. Environ Earth Sci 78:45

Wang Q, Pan R, Jiang B, Li SC, He MC, Sun HB, Wang L, Qin Q, Yu HC, Luan YC (2017) Study on failure mechanism of roadway with soft rock in deep coal mine and confined concrete support system. Eng Fail Anal 81:155–177

Wang Q, Jiang B, Pan R, Li SC, He MC, Sun HB, Qin Q, Yu HC, Luan YC (2018) Failure mechanism of surrounding rock with high stress and confined concrete support system. Int J Rock Mech Min Sci 102:89–100

Wu DY, Qin S (2020) Loose and broken distribution of soft coal-rock in deep coal roadway sidewall. Geotech Geol Eng. https://doi.org/10.1007/s10706-020-01337-y

Wu GJ, Chen WZ, Jia SP, Tan XJ, Zheng PQ, Tian HM, Rong C (2020) Deformation characteristics of a roadway in steeply inclined formations and its improved support. Int J Rock Mech Min Sci 130:104324

Wu WD, Bai JB, Wang XB, Yan S, Wu SX (2019) Numerical study of failure mechanisms and control techniques for a gob-side yield pillar in the Sijiazhuang Coal Mine, China. Rock Mech Rock Eng 52:1231–1245

Xie HP, Gao MZ, Zhang R, Peng GY, Wang WY, Li AQ (1000m) Study on the mechanical properties and mechanical response of coal mining at 1000m or deeper. Rock Mech Rock Eng 52:1475–1490

Xu C, Fu Q, Wang K, Guo CF, Li XF (2020) Effects of the deviatoric stress ratio on the coal failure and permeability during deep mining. Geotech Geol Eng. https://doi.org/10.1007/s10706-020-01417-z

Xu F, Li SC, Zhang QQ, Li LP, Shi SP, Zhang Q (2017) A new type support structure introduction and its contrast study with traditional support structure used in tunnel construction. Tunn Undergr Sp Tech 63:171–182

Yang SQ, Chen M, Jing HW, Chen KF, Meng B (2017) A case study on large deformation failure mechanism of deep soft rock roadway in Xin'An coal mine, China. Eng Geo 217:89–101

Yardimci AG, Karakus M (2020) A new protective destressing technique in underground hard coal mining. Int J Rock Mech Min Sci 130:104327

Yoo C (2016) Effect of spatial characteristics of a weak zone on tunnel deformation behavior. Geomech Eng 11:41–58

Zhang N, Li BY, Li GC, Qian DY, Yu XY (2013) Inhomogeneous damage and sealing support of roadways through thin bedded coal-rock crossovers. J Min Saf Eng 30:1–6 (in Chinese)

Zheng SB (2010) 3D geostress field distribution and roadway layout optimization in Sihe Mine. J China Coal Soc 35(05):717–722 (in Chinese)